Brownian diffusion of ion channels in different membrane patch geometries

Fang Wei, Dongping Yang, Ronny Straube, and Jianwei Shuai

Brownian Diffusion of Ion Channels in Different Membrane Patch Geometries

Fang Wei[1], Dongping Yang[1], Ronny Straube[2] *, and Jianwei Shuai[1] †

[1]*Department of Physics and Institute of Theoretical Physics and Astrophysics*
Xiamen University, Xiamen 361005, China
[2]*Max Planck Institute for Dynamics of Complex Technical Systems,*
Systems Biology Group, Sandtorstr. 1,
D-39106 Magdeburg, Germany

We asymptotically calculate the spatially averaged mean first passage time (MFPT) of a diffusing channel protein in a finite membrane patch containing a small absorbing anchor site. Different two-dimensional membrane geometries are considered including a circular, a square-shaped, a rectangular and a cylindrical domain. The asymptotic expressions are found to be in excellent agreement with results from Monte-Carlo simulations if the radius of the diffusing protein is sufficiently small. For a larger radius a simple correction to the asymptotic expressions is proposed. We show that the average MFPT for a circle and a square-shaped domain of the same area are approximately equal as long as the anchor site is close to the center of the domain. We also discuss how the average MFPT depends on the aspect ratio of a rectangular and a cylindrical domain. Among such domains with a fixed area a minimal MFPT is obtained for the square-shaped domain.

Keywords: Mean first passage time, Ion channel, Brownian diffusion, IP$_3$R, Neumann function

PACS numbers:

I. INTRODUCTION

Cytosolic calcium ions (Ca^{2+}) play a crucial role in the regulation of various physiological phenomena, such as exocytosis, enzyme control, gene regulation, cell growth and proliferation, and apoptosis [1]. A common source of cytosolic Ca^{2+} in many cells is the release of Ca^{2+} through the inositol 1,4,5-trisphosphate receptor (IP$_3$R) from intracellular stores, e.g. the endoplasmic reticulum (ER), in response to the second messenger inositol 1,4,5-trisphosphate (IP$_3$) [2]. Thus, the spatial distribution of IP$_3$Rs can be important for the local delivery of Ca^{2+} to specific sites within the cell to regulate Ca^{2+}-dependent subcellular functions [3, 4].

In many cell types IP$_3$R is diffusible within the ER membrane, and it can dynamically migrate upon cell stimulation. For example, long term agonist stimulation in the smooth muscle cell line A7r5 leads to a global re-distribution of type-1 IP$_3$Rs [5]. In addition to the global movements of IP$_3$Rs, it has been observed that local clustering of IP$_3$Rs can occur, for example, in the basophilic cell line RBL-2H3 where IP$_3$R clustering can be rapidly triggered by activation of the Ca^{2+} signalling cascade [6], and IP$_3$R clustering is not dependent on changes in the structure of the ER [7]. Also, the maturation of oocytes before fertilization leads to IP$_3$R clustering [8].

The biological consequences of IP$_3$R clustering are not clear yet. Clustered IP$_3$Rs show a strong stochastic open/close dynamics causing a noisy Ca^{2+} signal.

Within a lattice model it has been shown that channel clusters can generate a stochastic backfiring pattern [9]. Other simulations suggest that the clustering distribution of IP$_3$Rs may improve the periodicity of local Ca^{2+} signals [10] and enhance the sensitivity of global Ca^{2+} signals responding to a weak IP$_3$ stimulus [11]. Based on global spiking data of four cell types, it was suggested that Ca^{2+} spikes are caused by random wave nucleation events with a regular regime arising from the array enhanced coherence resonance effect of IP$_3$R clusters [12].

The dynamical regulation of IP$_3$R clustering has been investigated only recently. First, it was suggested that Ca^{2+} triggered the clustering of IP$_3$Rs [6]. Theoretical analysis showed that a periodic (Ca^{2+}) signal could lead to an oscillatory or to a quasi-stationary cluster size distribution [13]. Later, it was shown that a conformational change in the IP$_3$R, evoked by IP$_3$, was sufficient to induce clustering [14]. Further experiments indicated that the depletion of the Ca^{2+} store may facilitate the clustering of IP$_3$Rs [15]. More recently, with patch-clamp recordings from the outer nuclear envelope of DT40 cells expressing rat IP$_3$R1 or IP$_3$R3, it was shown that IP$_3$ causes IP$_3$R rapidly and reversibly to aggregate into small clusters of about four IP$_3$Rs [16]. However, another study indicated that puff sites represent preestablished stable clusters of IP$_3$Rs and that functional IP$_3$Rs are not readily diffusible within the ER membrane in SH-SY5Y, Hela and astrocyte cells [17].

These experiments clearly demonstrate the need to reliably estimate the time scale on which clustering occurs. In general, one can expect an effect of IP$_3$R clustering on the Ca^{2+} dynamics when the time scale for clustering and the time scale for the open/closing dynamics of individual IP$_3$R channels are comparable. To estimate the time scale of IP$_3$R clustering we assume that IP$_3$Rs undergo

Brownian motion on an ER membrane patch containing an anchor site. This could be, for example, a fixed cytoskeletal structure which traps and fixes the IP$_3$R channels upon encounter. The relevant time scale for clustering is given by the mean first passage time (MFPT) [18], i.e. the average time it takes an IP$_3$R channel to reach a given target site on the membrane for the first time. In the case that clustering is a purely diffusion-limited process the MFPT can be calculated in the framework of the Smoluchowski theory [19].

The MFPT arises in many applications, but explicit results were mostly restricted to one-dimensional geometries [20–23]. Recently, first results were given for the MFPT in more complex geometries including microdomains [24], two- and three dimensional domains containing small exit sites [25–28, 30], as well as for regular lattices [31] and complex networks [32, 33]. Specifically, in a bounded two-dimensional domain containing a circular trapping region the MFPT can be expressed in terms of the Neumann function G_N as [28, 29]

$$T_{x_0}(x) = -\frac{|\Omega|}{D} G_N(x; x_0) \qquad (1)$$

where x and x_0 denote the starting point for the random walk inside Ω and the center of the trapping region, respectively. $|\Omega|$ and D correspond to the area of the domain and the diffusion coefficient, respectively.

In two dimensions the Neumann function has the general form

$$G_N(x; x_0) = -\frac{1}{2\pi} \ln |x - x_0| + R_N(x; x_0) \qquad (2)$$

where R_N represents the regular part of G_N at x_0 which is uniquely determined by the boundary value problem

$$\begin{aligned} \Delta G_N &= \frac{1}{|\Omega|} - \delta(x - x_0), \quad x \in \Omega \\ \partial_n G_N &= 0, \quad x \in \partial\Omega \\ \int_\Omega dx\, G_N &= 0\,. \end{aligned} \qquad (3)$$

Here, Δ denotes the Laplace operator in two dimensions and ∂_n denotes the derivative in the direction of the outward normal of the respective domain. The spatially averaged MFPT ($\bar{T}$) of Eq. 1 is then given in terms of $R_N(x; x_0)$ as

$$\bar{T}_{x_0} = \frac{|\Omega|}{D} \left(\frac{1}{2\pi} \ln \frac{L_c}{\varepsilon} + \lim_{x \to x_0} R_N(x; x_0) \right) \qquad (4)$$

where L_c denotes a characteristic length scale of the domain Ω and ε is the effective radius of the trapping region. It accounts for the fact that the diffusing ion channel (radius r_{ch}) is immediately absorbed upon the first contact with the anchor site (radius r_{an}). Thus $\varepsilon = r_{ch} + r_{an}$. Note that in the continuum description the diffusing channel is treated as a point particle.

Often, the leading order term in Eq. 4 is sufficient to estimate the order of magnitude for the average MFPT,

and it only requires knowledge of three parameters: The total surface area $|\Omega|$, the diffusion coefficient D and the effective radius of the trapping region relative to the characteristic length scale of the domain ε/L_c. Thus the leading order term is insensitive to geometrical details of the underlying domain. If more than one length scale is required to characterize the shape of the domain, such as the aspect ratio of a rectangular domain, then the $O(1)$ term, involving the regular part of the Neumann function, can become important especially in highly asymmetric domains [26].

Strictly speaking, the expressions in Eqs. 1, 3 and 4 are valid only in the asymptotic limit $\varepsilon \ll L_c$, but comparison with numerical solutions of the respective partial differential equations gave excellent agreement up to values of $\varepsilon/L_c = 0.2$ [26, 28]. In the present work, we compare the asymptotic expression for the spatially averaged MFPT (Eq. 4) with direct Monte Carlo simulations of a Brownian particle (IP$_3$R channel) in different two-dimensional domains. We study in detail its dependence on the size of IP$_3$R channel, the size and the position of the anchor site, the size of the ER membrane patch, and different membrane shapes.

We find excellent agreement between the asymptotic expression in Eq. 4 and stochastic simulations if the $O(1)$ term is taken into account and the radius of the diffusing channel (r_{ch}) is sufficiently small. For a larger channel radius a simple correction to Eq. 4 is proposed which is in very good agreement with the results of stochastic simulations. We also investigate how the average MFPT depends on the aspect ratio of a rectangular and a cylindrical domain. Among such domains with a fixed area a minimal MFPT is obtained for a square-shaped domain.

II. SIMULATION METHOD

We consider Brownian diffusion of an IP$_3$R channel in different two-dimensional ER membrane geometries including a circular, a square-shaped, a rectangular and a cylindrical domain. For the first three domains we use reflecting boundary conditions while the cylindrical domain is modelled as a rectangular domain with periodic boundary conditions along the y-axis and reflecting boundary conditions along the x-axis.

The IP$_3$R is represented as a small particle with a radius of r_{ch} that diffuses within the ER membrane with diffusion coefficient D. Based on electron microscopy and single particle analysis of purified IP$_3$R, the radius of a channel was estimated in the range 9 nm to 18 nm [34]. Using fluorescence recovery after photobleaching it was suggested that IP$_3$Rs diffusion within ER membranes is with a diffusion coefficient D of 0.03-0.04 μm^2/s [35] or 0.45 μm^2/s [36].

In the simulation, the IP$_3$R channel undergoes a Brownian random walk in both x and y directions. Their positions are updated at time steps Δt by adding random numbers drawn from a Gaussian distribution with zero

mean [17]. The width (standard deviation) of the Gaussian is $\sqrt{2D\Delta t}$. In the simulation, we chose the time step $\Delta t = 5 \times 10^{-5}$ s. Different time steps have been tested giving the same results.

We also consider an anchor site or absorbing region with radius r_{an} in the patch representing a fixed cytoskeletal structure to trap the channels. The fixed anchor site is designated as IP$_3$R channel trap location. Here we assume r_{an} is of order of 10 nm [17]. An IP$_3$R channel moving within a distance of $\varepsilon = r_{ch}+r_{an}$ will become trapped at the anchor site. To remain compatible with the assumptions for the derivation leading to Eq. 4, we assume that trapped channels will neither affect the trap diameter nor its location. When the channel reaches the patch boundary within a distance which is less than r_{ch}, reflecting boundary conditions will be used for the mobile IP$_3$R.

In the simulation, the IP$_3$R channel is located in the patch randomly at the beginning. Then the channel undergoes a Gaussian random walk with diffusion coefficient D. The random diffusing time of the channel before colliding with the anchor site is calculated. A spatially averaged MFPT is defined as the average of the diffusion times obtained from 500,000 trials starting at arbitrary positions in the patch.

III. RESULTS

A. IP$_3$R diffusion in a circular patch

We consider a diffusing particle in a circular domain of radius R containing a small absorbing circular region of effective radius ε at the center. The diffusion coefficient of the particle is D. Then the MFPT required for the particle to hit the absorbing region at the center when starting at an arbitrary position inside the annulus $\varepsilon < r < R$ is determined by the simple boundary value problem

$$
\begin{aligned}
\Delta T &= -\frac{1}{D}, \quad \varepsilon < r < R \\
T &= 0, \quad r = \varepsilon \\
\partial_r T &= 0, \quad r = R
\end{aligned}
\tag{5}
$$

Due to the spherical symmetry the problem can be solved analytically. We include it here for didactical purpose since it will serve as a benchmark for more complicated geometries considered later. The solution of Eqs. 5 gives the MFPT as

$$
T(r) = \frac{\varepsilon^2 - r^2}{4D} + \frac{R^2}{2D} \ln \frac{r}{\varepsilon}.
\tag{6}
$$

Then the spatially averaged MFPT is computed as

$$
\begin{aligned}
\bar{T}_{circ} &= \frac{1}{\pi(R^2 - \varepsilon^2)} \int_0^{2\pi} d\varphi \int_\varepsilon^R T(r)r\,dr \\
&= \frac{R^2}{2D} \ln \frac{R}{\varepsilon} - \frac{3}{8}\frac{R^2}{D} + \mathcal{O}\left(\frac{\varepsilon^2}{R^2}\ln \frac{R}{\varepsilon}\right).
\end{aligned}
\tag{7}
$$

In typical applications the contact radius ε is in the nanometer range whereas diffusion occurs in membrane patches with a typical length scale in the micrometer range. In that case terms of $\mathcal{O}((\varepsilon^2/R^2)\ln(R/\varepsilon))$ and smaller can be neglected in Eq. 7 and the spatially averaged MFPT is well approximated by

$$
\bar{T}_{circ} \approx \frac{R^2}{2D} \ln \frac{R}{\varepsilon} - \frac{3}{8}\frac{R^2}{D}.
\tag{8}
$$

To compare this expression with the general form of the average MFPT shown in Eq. 4 we rewrite Eq. 8 as

$$
\bar{T}_{circ} \approx \frac{\pi R^2}{D} \left(\frac{1}{2\pi} \ln \frac{R}{\varepsilon} - \frac{3}{8\pi} \right)
$$

which shows that the regular part of the Neumann function for a circular domain with a singularity at the origin is given by $R_{N,circ}(0) = -3/8\pi$ [37].

Now with the Brownian random walk simulation, we consider a diffusing IP$_3$R channel in a circular domain of radius R_{circ} with a reflecting boundary and containing a small absorbing circular region of radius r_{an} at the center. The radius of the channel is r_{ch} and its diffusion coefficient is D.

First we discuss the first passage time (FPT) for the channel starting at a given distance r. As shown in Figure 1A the FPTs exhibit an exponential distribution with a time constant of $T = 41.7$s at $r = 1\mu$m corresponding to the MFPT. For the exponential distribution, the standard deviation of the FPTs is equal to its mean and Eq. 6 yields $T = 42.1$s with $\varepsilon = r_{an} + r_{ch}$ and $R = R_{circ}$. Figure 1B shows excellent agreement of the MFPT between the stochastic simulation and Eq. 6 as function of the distance r.

In the following, we focus on the discussion of the spacially averaged MFPT for a channel starting at arbitrary positions in the patch. As shown in Figure 1C the FPT still exhibits an exponential distribution with a time constant of $\bar{T} = 40.6$s corresponding to the spatially averaged MFPT. For the example given in Figure 1C, using only the leading order term in Eq. 8 yields a spatially averaged MFPT of $\bar{T} = 49.1$s, while taking into account the contribution from the second order term in Eq. 8 significantly improves the result to 40.7s.

Figure 2 shows the results of stochastic simulations for the dependence of the spatially averaged MFPT on several parameters such as the diffusion coefficient D (Fig. 2A), the patch radius R_{circ} (Fig. 2B), the anchor radius r_{an} (Fig. 2C), and the channel radius r_{ch} (Fig. 2D), together with the asymptotic result in Eq. 8 with $R = R_{circ}$. For comparison we have also plotted the leading order term alone (dashed line) in Figure 2. Figs. 2A-C clearly demonstrate the importance of the $O(1)$ term in Eq. 4 ($\sim R_N$) to achieve full agreement between the results from stochastic simulations and the two-term approximation in Eq. 8 even in the case $\varepsilon/R = (r_{ch} + r_{an})/R \ll 1$.

Figure 2D shows marked deviations between the results of the stochastic simulation and the asymptotic result
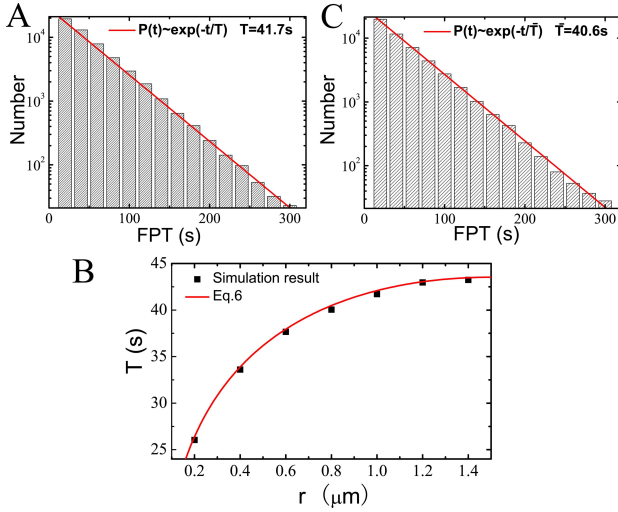
FIG. 1: (Color online) The FPT for a Brownian IP$_3$R channel in a circular patch with an anchor site at its center. (A) Exponential distribution of the FPT for a channel starting at a given distance $r = 1\mu$m. (B) The MFPT as a function of the distance r. Black squares are stochastic simulation data; Red solid line denotes the theoretical result in Eq. 6 with $R = R_{circ}$. (C) Exponential distribution of the FPT for a channel starting at arbitrary positions in the patch. Parameters are $r_{an} = 10$nm, $r_{ch} = 9$nm, $R_{circ} = 1.5\mu$m and $D = 0.1\mu$m^2/s. The distribution can be fitted by a straight line with a slope of 40.6s.

FIG. 2: (Color online) Average MFPT for a diffusing IP$_3$R channel in a circular patch with an anchor site of radius r_{an} at its center. (A) $1/\bar{T}$ as a function of D at $r_{ch} = 9$ nm, $r_{an} = 10$ nm and $R_{circ} = 1.5$ μm; (B) $\bar{T}$ as a function of R_{circ} at $r_{ch} = 9$ nm, $r_{an} = 10$ nm and $D = 0.1$ μm^2/s; (C) $\bar{T}$ as a function of r_{an} at $R_{circ} = 1.5$ μm, $r_{ch} = 9$ nm and $D = 0.1$ μm^2/s; (D) $\bar{T}$ as a function of r_{ch} at $R_{circ} = 1.5$ μm, $r_{an} = 10$ nm and $D = 0.1$ μm^2/s. Black symbols are stochastic simulation data; Red solid lines denote theoretical results in Eq. 8 with $R = R_{circ}$; Blue dashed lines denote the leading order term of Eq. 8. The green dash-dotted line in D denotes the theoretical result in Eq. 8 with $R = R_{circ} - r_{ch}$.

(red curve) in Eq. 8 with $R = R_{circ}$ as the radius (r_{ch}) of the diffusing channel protein increases. However, when the true radius of the domain R is replaced by an effective radius $R = R_{circ} - r_{ch}$, we again find excellent agreement (green curve) between the results of the stochastic simulation and the asymptotic result in Eq. 8. This suggests the following interpretation: In contrast to the derivation of the asymptotic result, the diffusing channel in the stochastic simulations is not treated as a point particle. Due to the reflecting boundary condition, it only samples an area with an effective radius of $R_{circ} - r_{ch}$ since it never penetrates the boundary region $(R_{circ} - r_{ch}, R_{circ}]$. As Figure 2 D shows this finite size effect becomes noticable already for comparably small values of $r_{ch}/R_{circ} \approx 0.01$.

B. IP$_3$R diffusion in a square patch

Now we consider a particle diffusing in a square domain Q_L^ε with a circular trapping region at the center. Here $Q_L^\varepsilon = Q_L \setminus C_\varepsilon$ where

$$Q_L = \{(x,y) : -L \leq (x,y) \leq L\}$$

is a square-shaped domain of length $2L$ and

$$C_\varepsilon = \{(x,y) : x^2 + y^2 \leq \varepsilon^2\}$$

denotes the circular trapping domain of effective radius $\varepsilon < L$ which is centered at the origin.

Then the MFPT is determined by

$$
\begin{aligned}
\Delta T &= -\frac{1}{D}, \quad (x,y) \in Q_L^\varepsilon \\
T &= 0, \quad (x,y) \in \partial C_\varepsilon \\
\partial_n T &= 0, \quad (x,y) \in \partial Q_L.
\end{aligned}
$$

Due to the different symmetry of the square and the absorbing circular region this problem can not be solved analytically. However, we know already that in the limit $\varepsilon \ll L$ the asymptotic solution has the form (cf. Eq. 4)

$$T(x,y) = -\frac{4L^2}{D}G_N(x,y) + \bar{T}_{sq}$$

where G_N is the Neumann function for the unit square and the average MFPT is given by

$$\bar{T}_{sq} = \frac{4L^2}{D}\left(\frac{1}{2\pi}\ln\frac{L}{\varepsilon} + \frac{1}{12} - \frac{1}{2\pi}\ln\pi\right). \qquad (9)$$

Here we have used the known result for the regular part of the Neumann function for the unit square [26]

$$\lim_{(x,y)\to(0,0)} R_{N,sq}(x,y) \approx \frac{1}{12} - \frac{1}{2\pi}\ln\pi.$$

Figure 3 shows the results of Monte Carlo simulations for the average MFPT of an IP$_3$R channel diffusing in a square patch of length L_{sq} with an anchor site in the center and reflecting boundary condition. We investigate the
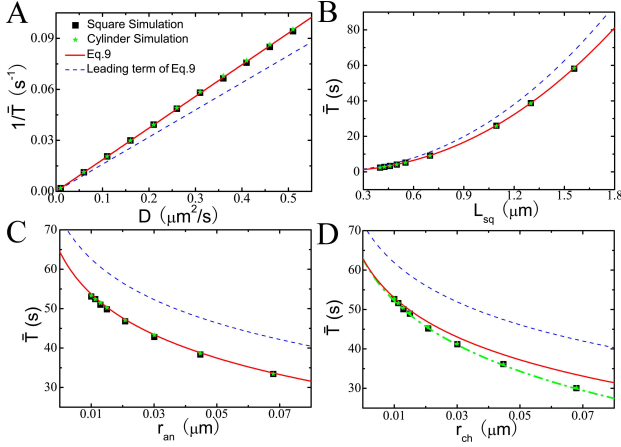
FIG. 3: (Color online) Spatially averaged MFPT for a diffusing IP$_3$R channel in a square domain and a square-shaped cylinder domain. Square symbols are simulation data for square domain; Star symbols are simulation data for square-shaped cylinder with $H_{cyl} = \pi R_C = L_{sq}$. (A) $1/\bar{T}$ as a function of D at $r_{ch} = 9$ nm, $r_{an} = 10$ nm, and $L_{sq} = 1.5$ μm; (B) $\bar{T}$ as a function of L_{sq} (or H_{cyl}) at $r_{ch} = 9$ nm, $r_{an} = 10$ nm, and $D = 0.1$ μm^2/s; (C) $\bar{T}$ as a function of r_{an} at $r_{ch} = 9$ nm, $D = 0.1$ μm^2/s, and $L_{sq} = 1.5$ μm and (D) $\bar{T}$ as a function of r_{ch} at $r_{an} = 10$ nm, $D = 0.1$ μm^2/s, and $L_{sq} = 1.5$ μm. Red solid lines correspond to theoretical results in Eq. 9 with $L = L_{sq}$; Blue dashed lines denote the leading order term of Eq. 9. The green dash-dotted line in D corresponds to the theoretical result in Eq. 9 with $L = L_{sq} - r_{ch}$.

dependence of the average MFPT on several parameters such as the diffusion coefficient D (Fig. 3A), the patch half-size L_{sq} (Fig. 3B), the anchor radius r_{an} (Fig. 3C), and the channel radius r_{ch} (Fig. 3D), respectively. Similar as for the circular domain, Figs. 3A-C show excellent agreement between numerical simulations and the asymptotic result for the average MFPT in Eq. 9 (with $L = L_{sq}$ and $\varepsilon = r_{an} + r_{ch}$) provided that $r_{ch}/L < 0.01$. However, Figure 3D also indicates that, to obtain quantitative agreement for increasing values of r_{ch}, we have to replace the true length of the square domain $L = L_{sq}$ by the effective length $L = L_{sq} - r_{ch}$ in Eq. 9.

Next we compare the average MFPT for a circular and a square patch having the same total area. For this purpose we set $L = R\sqrt{\pi}/2$ in Eq. 9 and obtain

$$
\begin{aligned}
T_{sq} &= \frac{\pi R^2}{D} \left(\frac{1}{2\pi} \ln \frac{\sqrt{\pi}R}{2\varepsilon} + \frac{1}{12} - \frac{1}{2\pi} \ln \pi \right) \\
&= \frac{\pi R^2}{D} \left(\frac{1}{2\pi} \ln \frac{R}{\varepsilon} - \frac{3}{8\pi} \left(\frac{2}{3} \ln(4\pi) - \frac{2\pi}{9} \right) \right) \\
&\simeq T_{circ}
\end{aligned}
$$

since $(2/3)\ln(4\pi) - 2\pi/9 \approx 1$. Hence, with respect to the $O(1)$ expansions in Eqs. 8 and 9 the average MFPT for a circular and a square domains of the same total area are basically indistinguishable. We have confirmed this result by stochastic simulations of the average MFPT for varying domain sizes as shown in Fig. 4.
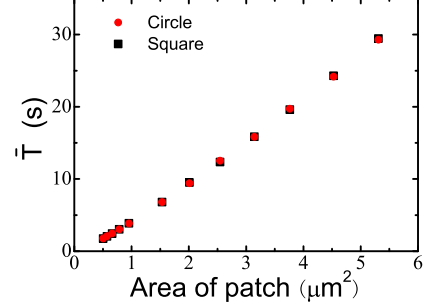
FIG. 4: (Color online) Dependence of the spatially averaged MFPT on the domain area. Red circle symbols are for circular domain and black square symbols are for square domain. Parameters are: $r_{ch} = 9$nm, $r_{an} = 10$nm and $D = 0.1\mu$m^2/s.

C.   IP$_3$R diffusion in a cylindrical patch

Biologically, the ER is more like a complex tubular network of small interconnected cylindrical membrane patches. Therefore, we consider now diffusion of IP$_3$R channels on a cylindrical domain of height $2H$ and radius R_C. However, in the simulations we neglect the curvature of the membrane since the size of an IP$_3$R channel is much smaller than the length and the circumference of the cylinder. Consequently, the membrane is assumed to be locally flat which can be modeled as a rectangular domain with periodic boundary conditions at $x = \pm \pi R_C$ and reflecting boundary conditions at the bottom and at the top boundaries of the cylinder at $y = \pm H$.

To obtain an expression for the average MFPT for a cylindrical domain we only have to replace the regular part of the Neumann function for the square in Eq. 9 with that for a cylindrical domain (height $2H$ and circumference $2\pi R_C$). In Ref. [26] we have derived two (alternative) expressions for this quantity given by

$$
\begin{aligned}
R_{N,cyl}(0,0) &= \frac{1}{2\pi} \left(\frac{H}{6R_C} - \ln \frac{H}{R_C} \right) \\
&\quad - \frac{1}{\pi} \sum_{n=1}^{\infty} \ln \left(1 - e^{-2n\frac{H}{R_C}} \right) \quad (10)
\end{aligned}
$$

or

$$
\begin{aligned}
R_{N,cyl}(0,0) &= \frac{1}{2\pi} \left(\frac{\pi^2 R_C}{6H} - \ln \pi \right) \\
&\quad - \frac{1}{\pi} \sum_{n=1}^{\infty} \ln \left(1 - e^{-2n\pi^2 \frac{R_C}{H}} \right). \quad (11)
\end{aligned}
$$

As we have shown in Ref. [26] both expressions represent the same function. However, the infinite sums possess a different speed of convergence. While the infinite sum in Eq. 10 rapidly converges for $H \gg R_C$ the infinite sum in Eq. 11 converges rapidly in the opposite limit.

Specifically, for $H \gg R_C$, the infinite sum in Eq. 10 can be neglected and the average MFPT for the cylindrical domain can be approximated as

$$\bar{T}_{cyl} \approx \frac{4\pi R_C H}{2\pi D}\left(\ln\frac{H}{\varepsilon} + \frac{H}{6R_C} - \ln\frac{H}{R_C}\right) \quad (12)$$

Note that this expression reduces to Eq. 9 if $H/R_C = \pi$ while keeping $H = L$ fixed. Hence, the average MFPT for a square-shaped domain and that of an equally sized cylindrical domain should be equal. This was confirmed by the stochastic simulations (star symbols) shown in Fig. 3 where we used $H_{cyl} = \pi R_C = L_{sq}$.

Next we discuss how the average MFPT depends on the aspect ratio $x = H/\pi R_C$ of the cylindrical domain. Therefore, the total surface area A_{cyl} is kept constant. Note that for a fixed area and a given aspect ratio the height H and radius R_C are given by

$$H = \frac{\sqrt{A_{cyl}x}}{2} \quad \text{and} \quad R_C = \frac{1}{2\pi}\sqrt{\frac{A_{cyl}}{x}},$$

which allows to rewrite the average MFPT as

$$\bar{T}_{cyl} = \frac{A_{cyl}}{2\pi D}\left(\ln\frac{\sqrt{A_{cyl}x}}{2\varepsilon} + \frac{\pi x}{6} - \ln(\pi x)\right)$$
$$-\frac{A_{cyl}}{\pi D}\sum_{n=1}^{\infty}\ln\left(1 - e^{-2\pi n x}\right) \quad (13)$$

using Eq. 10 or

$$\bar{T}_{cyl} = \frac{A_{cyl}}{2\pi D}\left(\ln\frac{\sqrt{A_{cyl}x}}{2\varepsilon} + \frac{\pi}{6x} - \ln(\pi)\right)$$
$$-\frac{A_{cyl}}{\pi D}\sum_{n=1}^{\infty}\ln\left(1 - e^{-2\pi n/x}\right) \quad (14)$$

using Eq. 11. Note that these expressions for the average MFPT are symmetric under the inversion $x \to 1/x$. Indeed, changing x to $1/x$ in Eq. 13 yields the expression in Eq. 14 and vice versa. For a quantitative comparison of these expressions with the results from numerical simulations we used a different number of terms (n_{max}) from the infinite sum in Eq. 13 to correctly reproduce the behavior of the average MFPT for $x \ll 1$.

As shown in Fig. 5 a minimal average MFPT is obtained for $x = 1$, i.e. for $H = \pi R_C$ corresponding to a square-shaped cylindrical domain. In general, we see a moderate dependence of the average MFPT on the aspect ratio. For example, increasing (or decreasing) the aspect ratio by a factor of 3 increases the average MFPT by approximately 13%. The asymptotic expression in Eq. 13 nicely fits the results of Monte-Carlo simulations given by the black symbols.

Since the Neumann function for a rectangular domain with reflecting walls and that for a cylindrical domain is the same as long as the singularity is located at the origin the average MFPT for both domains should also be equal.
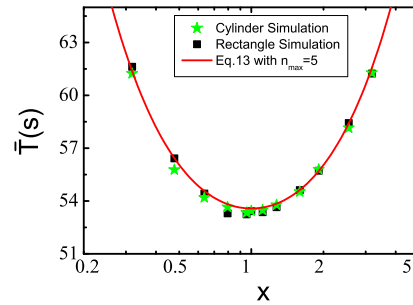
FIG. 5: (Color online) Dependence of the average MFPT on the aspect ratio $x = H/\pi R_C$ of a cylindrical domain (or on the ratio of x =width/length for a rectangular domain) with an anchor site ($r_{an} = 10$nm) at the center. The area of the respective domain is kept fixed at $A = 9\mu m^2$. Green star symbols represent simulation data for the cylindrical domain, black square symbols represent simulation data for the rectangular domain. The red curve corresponds to the theoretical result (Eq. 13) with $n_{max} = 5$, $D = 0.1\mu m^2$/s and $\varepsilon = 19$ nm.

To confirm this we plot in Fig. 5 the dependence of the average MFPT on the ratio between the width and the length of a rectangular domain with reflecting boundary conditions. Similarly as for the cylindrical domain, a minimal average MFPT is obtained when the aspect ratio equals one, i.e. for a square-shaped domain.

D. The case of an off-center anchor site

In the cases investigated so far the anchor site was always located at the center of the domain. Now we consider the situation when the anchor site is shifted away from the center by a distance d.

In principle, all one has to know is the regular part of the Neumann function for the respective domain, but with the singular point x_0 (cf. Eq. 3) shifted off the center. However, already for the case of a rectangular domain the explicit expression for the Neumann function with an off-center singularity is very clumpsy [38]. Therefore, to illustrate the general procedure we consider only the case of a circular domain with an off-center absorbing region. In that case the Neumann function (for the unit disk) has the explicit representation [37]

$$G_N(x, x_0) = \frac{1}{2\pi}\left(-\ln|x - x_0| - \ln\left|x|x_0| - \frac{x_0}{|x_0|}\right|\right)$$
$$+ \frac{1}{2\pi}\left[\frac{1}{2}\left(|x|^2 + |x_0|^2\right) - \frac{3}{4}\right].$$

Here, x denotes the normalized distance by R. The reg-

ular part of G_N is defined as (cf. Eq. 2)

$$R_N(x, x_0)$$
$$= G_N(x, x_0) + \frac{1}{2\pi} \ln |x - x_0|$$
$$= \frac{1}{2\pi} \left[-\ln \left| x |x_0| - \frac{x_0}{|x_0|} \right| + \frac{1}{2} \left(|x|^2 + |x_0|^2 \right) - \frac{3}{4} \right].$$

Hence, the average MFPT for an anchor site at an arbitrary point inside a circular domain becomes

$$\bar{T}_{circ}(x_0)$$
$$= \frac{\pi R^2}{D} \left(\frac{1}{2\pi} \ln \frac{R}{\varepsilon} + \lim_{x \to x_0} R_N(x, x_0) \right)$$
$$= \frac{R^2}{2D} \left(\ln \frac{R}{\varepsilon} - \left(\frac{3}{4} + \ln \left| x_0 |x_0| - \frac{x_0}{|x_0|} \right| - |x_0|^2 \right) \right).$$

Without loss of generality we assume that anchor site is shifted along the x-axis, i.e. $x_0 = (a, 0) = (d/R, 0)$. Then the expression for the average MFPT simplifies to

$$\bar{T}_{circ}(a) = \frac{R^2}{2D} \left(\ln \frac{R}{\varepsilon} - \frac{3}{4} - \left(\ln \left| a^2 - 1 \right| - a^2 \right) \right) \quad (15)$$

which reduces to Eq. 8 in the limit $a \to 0$.

The results of the stochastic simulations in Figure 6 show very good agreement with Eq. 15. For comparison we have also performed simulations in a square-shaped domain with reflecting boundary conditions and in a domain with cylindrical topology where $L_{cyl} = \pi R_C$, all having the same area. They indicate that the average MFPT becomes sensible for the shape of the domain as the absorbing anchor site is shifted towards the domain boundary. Specifically, marked deviations between the average MFPT for the circular and the square-shaped domain occur when $d/L_{sq} > 0.6$.

IV. DISCUSSION AND CONCLUSIONS

In this paper we combine asymptotic analytical methods with Monte Carlo simulations to discuss the Brownian movement of calcium ion channels (IP$_3$Rs) on a membrane patch of the endoplasmic reticulum (ER) containing a small absorbing anchor site to trap the channel. We find excellent agreement between the asymptotic expressions and stochastic simulations if the $O(1)$ in Eq. 4, coming from the regular part R_N of an associated Neumann function, is taken into account and the radius of the diffusing channel (r_{ch}) is sufficiently small.

As the channel radius increases one has to take into account that the diffusing channel only samples an effective area when reflecting boundary conditions are applied. Based on this observation we suggest a simple correction to the asymptotic expression for the average MFPT when the channel radius increases. Specifically, at large channel radius, the characteristic length of the domain L_c should be replaced by the effective length $L_c - r_{ch}$ in
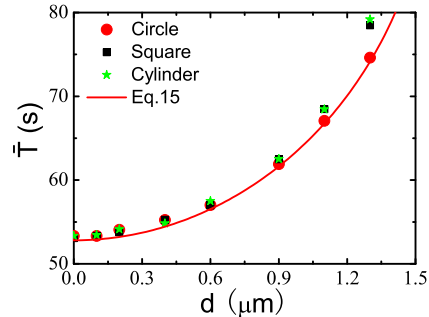
FIG. 6: (Color online) Dependence of the average MFPT on the distance d of the anchor site from the patch center for different domain shapes. Red circles represent simulation data for the circle patch with $R = 1.69$ μm; black squares represent simulation data for the square patch (all boundaries reflecting) with $L_{sq} = 1.5$ μm; green stars represent simulation data for the cylindrical patch with $L_{cyl} = 1.5\mu m = \pi R_C$. Here $r_{ch} = 9$ nm, $r_{an} = 10$ nm and $D = 0.1$ μm^2/s.

Eq. 4 keeping the functional form of the expression for the average MFPT the same.

Both asymptotic results and Monte Carlo simulations show that the average MFPT for a circular and a square-shaped domain of the same total area are indistinguishable if the anchor site remains within half a characteristic length scale from the domain center (Fig. 6). This suggests that in symmetric domains, which are characterized by only one length scale, the average MFPT is insensitive to the particular shape of the domain boundary if the trapping site is sufficiently close to the domain center.

However, when the domain is asymmetric, as in the case of a rectangular or a cylindrical domain, the average MFPT depends on the aspect ratio between the characteristic length scales of the respective domain. As a result, one can observe a difference in the average MFPT, compared to a square-shaped domain of the same area, even when the anchor site is located at the origin. Changing the aspect ratio can only increase the average MFPT compared to a square-shaped domain of the same area for which the average MFPT assumes a minimum.

In the present study we focused on the spatially averaged MFPT of a small diffusing channel protein towards a small absorbing anchor site in different two-dimensional geometries which was motivated by the observed clusering of IP$_3$R calcium channels diffusing within a finite ER membrane patch. However, we would like to mention that our results may also be useful to estimate the average MFPT of channel proteins or receptor molecules on other membrane structures or quasi two-dimensional cellular organelles. The inverse of the average MFPT can be used as an estimate for the diffusion-limited rate constant to describe the association between a diffusing channel protein and a preestablished static trapping site such as an IP$_3$R cluster.

V.   ACKNOWLEDGMENTS

VI.   REFERENCES

[1] M. J. Berridge. Nat. Rev. Mol. Cell Biol. *1* 11–21 (2000).

[2] J. K. Foskett, C. White, K. H. Cheung, and D. O. Mak. Physiol. Rev. *87* 593–658 (2007).

[3] K. Ito, Y. Miyashita, and H. Kasai. EMBO J. *16* 242–251 (1996).

[4] P. Thorn, K. E. Fogarty, and I. Parker. Proc. Natl. Acad. Sci. USA *101* 6774–6779 (2004).

[5] E. Vermassen, K. Van Acker, W. G. Annaert, B. Himpens, G. Callewaert, L. Missiaen, H. De Smedt, and J. B. Parys. J. Cell Sci. *116* 1269–1277 (2003).

[6] B. S. Wilson, J. R. Pfeiffer, A. J. Smith, J. M. Oliver, J. A. Oberdorf, and R. J. H. Wojcikiewicz. Mol. Biol. Cell *9* 1465–1478 (1998).

[7] M. Chalmers, M. J. Schell, and P. Thorn. Biochem. J. *394* 57–66 (2006).

[8] M. J. Boulware, and J. S. Marchant. Curr. Biol. *15* 765–770 (2005).

[9] M. Falcke, L. Tsimring, and H. Levine. Phys. Rev. E *62* 2636–2643 (2000).

[10] J. W. Shuai, and P. Jung. Phys. Rev. Lett. *88* 068102 (2002).

[11] J. W. Shuai, and P. Jung. Proc. Natl. Acad. Sci. USA *100* 506–510 (2003).

[12] A. Skupin, H. Kettenmann, U. Winkler, M. Wartenberg, H. Sauer, S. C. Tovey, C. W. Taylor, and M. Falcke. Biophys. J. *94* 2404–2411 (2008).

[13] R. Straube and M. Falcke. Phys. Rev. E *76* 010402(R) (2007).

[14] Y. Tateishi, M. Hattori, T. Nakayama, M. Iwai, H. Bannai, T. Nakamura, T. Michikawa, T. Inoue, and K. Mikoshiba. J. Biol. Chem. *280* 6816–6822 (2005).

[15] Y. Tojyo, T. Morita, A. Nezu, and A. Tanimura. J. Pharmacol. Sci. *107* 138–150 (2008).

[16] T.-U. Rahman, A. Skupin, M. Falcke, and C. W. Taylor. Nature *458* 655–659 (2009).

[17] I. F. Smith, S. M. Wiltgen, J. W. Shuai, and I. Parker. Science Signaling *2* ra77 1–7 (2009).

[18] S. Redner. A Guide to First-Passage Processes (Cambridge Univ. Press, Cambridge, UK, 2001)

[19] M. v. Smoluchowski. Z. Phys. Chem. *92* 129–168 (1917).

[20] S. H. Noskowicz and I. Goldhirsch. Phys. Rev. Lett. *61* 500–502 (1988).

[21] J. E. Fletcher, S. Havlin, and G. H. Weiss. J. Stat. Phys. *51* 215 (1988).

[22] A. Bar-Haim and J. Klafter. J. Chem. Phys. *109* 5187 (1998).

[23] M. Gitterman. Phys. Rev. E *62* 6065 (2000).

[24] Z. Schuss, A. Singer, and D. Holcman. Proc. Natl. Acad. Sci. USA *104* 16098–16103 (2007).

[25] A. Singer, Z. Schuss, and D. Holcman. J. Stat. Phys. *122* 491–509 (2006).

[26] R. Straube, M. J. Ward, and M. Falcke. J. Stat. Phys. *129* 377–405 (2007).

[27] O. Bénichou and R. Voituriez. Phys. Rev. Lett. *100* 168105 (2008).

[28] D. Coombs, R. Straube, and M. Ward. SIAM J. Appl. Math. *70* 302–332 (2009).

[29] S. Pillay, M. J. Ward, A. Peirce and T. Kolokolnikov. SIAM Multiscale Simul. Model. *8* 803–835 (2010).

[30] A. F. Cheviakov, M. J. Ward, and R. Straube. SIAM Multiscale Simul. Model. *8* 836–870 (2010).

[31] S. Condamin, O. Bénichou, and M. Moreau. Phys. Rev. Lett. *95* 260601 (2005).

[32] J. D. Noh and H. Rieger. Phys. Rev. Lett. *92* 118701 (2004).

[33] S. Condamin, O. Bénichou, V. Tejedor, R. Voituriez and J. Klafter. Nature *450* 77–80 (2007).

[34] C. W. Taylor, P. C. da Fonseca, and E. P. Morris. Trends Biochem. Sci. *29* 210–219 (2004).

[35] M. Ferreri-Jacobia, D.-O. D. Mak, and J. K. Foskett. J. Biol. Chem. *280* 3824–3831 (2005).

[36] K. Fukatsu, et al. J. Biol. Chem. *279* 48976–48982 (2004).

[37] T. Kolokolnikov, M. S. Titcombe, and M. J. Ward. Eur. J. Appl. Math. *16* 161–200 (2005).

[38] P. C. Bressloff, B. A. Earnshaw, and M. J. Ward. SIAM J. Appl. Math. *68* 1223–1246 (2008).